GGPP depletion initiates metaflammation through disequilibrating CYB5R3-dependent eicosanoid metabolism

Received for publication, June 28, 2020, and in revised form, August 20, 2020 Published, Papers in Press, September 10, 2020, DOI 10.1074/jbc.RA120.015020

Lisha Wei‡, Yan-Yan Zheng‡, Jie Sun, Pei Wang, Tao Tao, Yeqiong Li, Xin Chen, Yongjuan Sang, Danyang Chong, Wei Zhao, Yuwei Zhou, Ye Wang, Zhihui Jiang, Tiantian Qiu, Chao-Jun Li*, Min-Sheng Zhu*, and Xuena Zhang*

From the State Key Laboratory of Pharmaceutical Biotechnology, Model Animal Research Center and Medical School of Nanjing University and Nanjing Drum Tower Hospital Affiliated with Nanjing University Medical School, Nanjing University, Nanjing, China

Edited by Dennis R. Voelker

Metaflammation is a primary inflammatory complication of metabolic disorders characterized by altered production of many inflammatory cytokines, adipokines, and lipid mediators. Whereas multiple inflammation networks have been identified, the mechanisms by which metaflammation is initiated have long been controversial. As the mevalonate pathway (MVA) produces abundant bioactive isoprenoids and abnormal MVA has a phenotypic association with inflammation/immunity, we speculate that isoprenoids from the MVA may provide a causal link between metaflammation and metabolic disorders. Using a line with the MVA isoprenoid producer geranylgeranyl diphosphate synthase (GGPPS) deleted, we find that geranylgeranyl pyrophosphate (GGPP) depletion causes an apparent metaflammation as evidenced by abnormal accumulation of fatty acids, eicosanoid intermediates, and proinflammatory cytokines. We also find that GGPP prenylate cytochrome b_5 reductase 3 (CYB5R3) and the prenylated CYB5R3 then translocate from the mitochondrial to the endoplasmic reticulum (ER) pool. As CYB5R3 is a critical NADH-dependent reductase necessary for eicosanoid metabolism in ER, we thus suggest that GGPP-mediated CYB5R3 prenylation is necessary for metabolism. In addition, we observe that pharmacological inhibition of the MVA pathway by simvastatin is sufficient to inhibit CYB5R3 translocation and induces smooth muscle death. Therefore, we conclude that the dysregulation of MVA intermediates is an essential mechanism for metaflammation initiation, in which the imbalanced production of eicosanoid intermediates in the ER serve as an important pathogenic factor. Moreover, the interplay of MVA and eicosanoid metabolism as we reported here illustrates a model for the coordinating regulation among metabolite pathways.

In obesity and several metabolic disorders, altered production of many inflammatory cytokines, adipokines, lipid mediators, and signaling through a plethora of immune receptors and intracellular mediators have been complicated. Such a metabolically triggered inflammation is called metaflammation (1), and now it is usually represents a state of chronic low-grade inflammation as a response to metabolic or nutrient disruption from one or more sources. It has been well-demonstrated that metaflammation seriously impacts the progression of the diseases (2). Current knowledge shows that the integration of the metabolic and inflammatory signaling network occurs at multiple levels, but how the metabolic disorders start with inflammation have long been unclear. In light of the phenotypic association of the MVA pathway with inflammation/immunity (3), we hypothesized that the MVA pathway might be a metabolic pathway triggering metaflammation.

The MVA pathway is fundamental for cholesterol biosynthesis and acts as an essential lipid-lowering therapeutic target (4). This pathway begins with synthesis of 3-hydroxy-3-methylglutaryl-CoA (HMG-CoA) by HMG-CoA synthase and then conversion of the resultant HMG-CoA to mevalonic acid by HMG-CoA reductase (HMGCR), the rate-limiting enzyme of the MVA pathway. By over 20 subsequent enzyme reactions along this pathway, cholesterol is synthesized by the post-squalene pathway, and meanwhile several bioactive intermediaries and end products are produced by a nonsterol pathway. These nonsterol metabolites include isoprenoids, dolichol, ubiquinone, and isopentenyladenine. Among these metabolites, farnesyl diphosphate and GGPP are the primary forms of isoprenoids capable of modifying proteins (5). Protein prenylation is a class of lipid modification of proteins, in which the farnesyl diphosphate (15-carbon) or GGPP (20-carbon) isoprenoids are covalently added to conserved cysteine residues (*e.g.* CAA*X* and CC*XX*) at or near the C terminus of proteins. This modification enables the proteins to interact with membrane or other proteins (5) but usually does not affect protein stability and activity (6). There are reports showing that small GTPases, including RAS, RHO, and RAB may be prenylated and translocated to membrane (7, 8)

GGPP is produced by GGPPS with sequential condensation reactions of dimethylallyl diphosphate with three units of isopentenyl diphosphate, and geranygeranylate proteins by geranylgeranyltransferase I/II (GGTase I/II). As such a prenylation process is attenuated by MVA inhibition (9), the MVA pathway seems to be required for the protein prenylation. More than 100 proteins with the prenylation motif of GGPP have been identified so far (10), and the prenylated proteins participate in multiple processes, including tumorigenesis (11, 12), glucose metabolism (13, 14), apoptosis (15), and adipocyte browning (16). Based on clinical observations from the mevalonate kinase

This article contains supporting information.
‡These authors contributed equally to this work.
*For correspondence: Chao-Jun Li, licj@nju.edu.cn; Min-Sheng Zhu, zhums@nju.edu.cn; Xuena Zhang, zhangxn@nicemice.cn.

deficiency patients with the mevalonate kinase loss-of-function gene mutation, however, the syndromes caused by the impairment of the MVA pathway are primarily exhibited by autoinflammation and autoimmune disorders (3). We thus speculated that the MVA pathway served as an important regulator of sterile inflammation. This point is also supported by recent observations (17, 18).

HMGCR inhibitors such as statins are widely used as lipid-lowering drugs by down-regulating cholesterol synthesis (9). Several reports show that administration of these drugs preferentially impairs vascular smooth muscle and blood pressure (19–24). The vascular smooth muscle seems sensitive to the impairment of MVA pathway. In addition, there is accumulating evidence showing a close relation of vascular smooth muscle in metabolic inflammation (25, 26). We thus examined the role of GGPPS in vascular smooth muscle cells. By analyzing a mouse line with smooth muscle-specific deletion of *Ggps1*, we surprisingly found that the mutant mice displayed abnormal expression of the genes related to inflammation and immunity, along with a progressive apoptosis of vascular smooth muscle cells (VSMCs). The addition of exogenous GGPP was able to restore the apoptosis process *in vitro*. Moreover, the deletion of GGPPS resulted in a significant increase in polyunsaturated fatty acids, showing an impaired eicosanoid production. This effect was attributable to abolished prenylation of CYB5R3 and hence failed translocation from mitochondria to the ER pool. As CYB5R3 was a required reductase for maintaining the microsomal oxidation/reduction environment necessary for eicosanoid metabolism, we concluded that GGPP produced by the MVA pathway essentially regulated eicosanoids homeostasis. As the eicosanoids are closely related to inflammation and immunity, our result reveals a link of MVA or cholesterol biosynthesis with metaflammation.

Results

MVA metabolism and GGPPS expression in postnatal aorta smooth muscle

In postnatal animals, to adapt to new environments such as milk nutrition and developmental requirements, such tissues as blood vessels remodel their metabolic programs. Among these programs, cholesterol biosynthesis is particularly important for synthesis of membrane material necessary for cell proliferation. We first measured MVA-associated genes in developing aorta smooth muscle tissues by a real-time PCR assay. From embryonic day 18.5 to adulthood, *Ggps1*, farnesyl diphosphate synthase (*Fdps*), and *Hmgcr* genes were expressed at a relatively constant level. The maximum difference was within 4-fold (Fig. 1*A*), showing the important role of MVA metabolism during aorta smooth muscle development. The expression of *Ggps1* was especially stable until day 25. We also measured the genes related to glycolysis (*Hk2*, *Pfkp* (platelet phosphofructokinase), *Ldhb* (lactate dehydrogenase B), and *Pdk2* (pyruvate dehydrogenase kinase isoform 2)), lipolysis (*Lpl*), β-oxidation (*Cpt1a* (carnitine palmitoyltransferase 1A) and *Acadl* (acyl-coenzyme A dehydrogenase)), lipogenesis (*Fasn*), and mitochondrial oxidation (*Cox4i1* and *Cox7a1* (cytochrome c oxidase subunit 4I1 and 7A1, respectively)). The expression levels of glucose and lipid metabolism–associated genes showed significant change with development and each played an important role at different stages (Fig. 1, *B–D*).

Expression of GGPPS in smooth muscle is required for the survival of neonatal mice

To determine the role of GGPP/GGPPS *in vivo*, we established a line with smooth muscle–specific deletion of *Ggps1* gene by crossing $Ggps1^{flox/flox}$ mice with SMA-Cre mice. The resultant $Ggps1^{flox/flox}$; *SMA-Cre*+ ($Ggps1^{SMKO}$) mice were used as knockout (KO) mice and $Ggps1^{flox/flox}$; SMA-Cre− or $Ggps1^{flox/+}$; SMA-Cre− mice were used as control (CTR) mice (Fig. 2*A*). A GGPPS expression in KO aorta declined up to 90% compared with CTR aorta while GGPPS expression in KO jejunum declined only 60% compared with CTR jejunum (Fig. 2, *B* and *C*). The birth of KO and CTR pups obeyed Mendelian ratio, but the KO pups started to die from 5 weeks after birth (Fig. 2*E*). The body weights of KO mice at 6 weeks were slightly reduced (CTR (21.71 ± 2.78 g) *versus* KO (18.47 ± 3.18 g), $p < 0.05$) (Fig. 2*D*). Macrophenotypic examination for the mutant mice showed normal morphologies of the main organs, including brain, lung, gut, bladder, airway, liver, and skeletal muscle (Fig. S1, *A–C* and *F–J*). The mutant hearts appeared slightly larger, but their histology and function show no apparent alteration (Fig. S1*E* and Table S1). To our surprise, the systolic blood pressure (SBP) of the KO mice at 7 weeks old was significantly reduced (from 116 ± 6.61 mm Hg of CTR to 66 ± 11.86 mm Hg; $p < 0.0001$) (Fig. 2*F*). Such a low SBP might cause severe cardiovascular disease and death (27, 28). In addition, no aorta aneurysm phenotype was observed in the mutant mice (Fig. S1*D*). Thus, our observation indicates that that the hypotension induced by GGPPS deletion may be the leading cause of animal death.

GGPPS deletion impairs artery smooth muscle cells by depletion of GGPP

As blood pressure may be regulated by VSMC contraction (29), the low blood pressure of GGPPS KO mice prompted us to examine the contractile properties of artery smooth muscle. To our surprise, for the mesentery from 7-week-old mice, the contractile responses to KCl depolarization and agonists (norepinephrine (NE) and U46619) were almost abolished (Fig. 2*G*). Smooth muscle contraction depends on the expression of contractile proteins, such as SMA, smooth muscle myosin heavy chain (SMMHC), and calponin. Immunofluorescent staining with anti-SMA antibody showed no expression of contractile proteins in the 7-week-old mutant aorta (Fig. 3*C*). More surprisingly, there were no DAPI signals in smooth muscle layer, indicating that no smooth muscle cells existed within the tissue (Fig. 3*C*). Hematoxylin and eosin (HE) staining also supported this conclusion (Fig. 3*E*). To find the point at which the smooth muscle cells started to decrease, we tested the aorta smooth muscle morphology at diverse ages. Before 3 weeks after birth, the mutant aorta tissues had normal smooth muscle cells and regular elastic lines, whereas the mutant aorta from 3-week-old mice had fewer smooth muscle cells, and the elastic lines

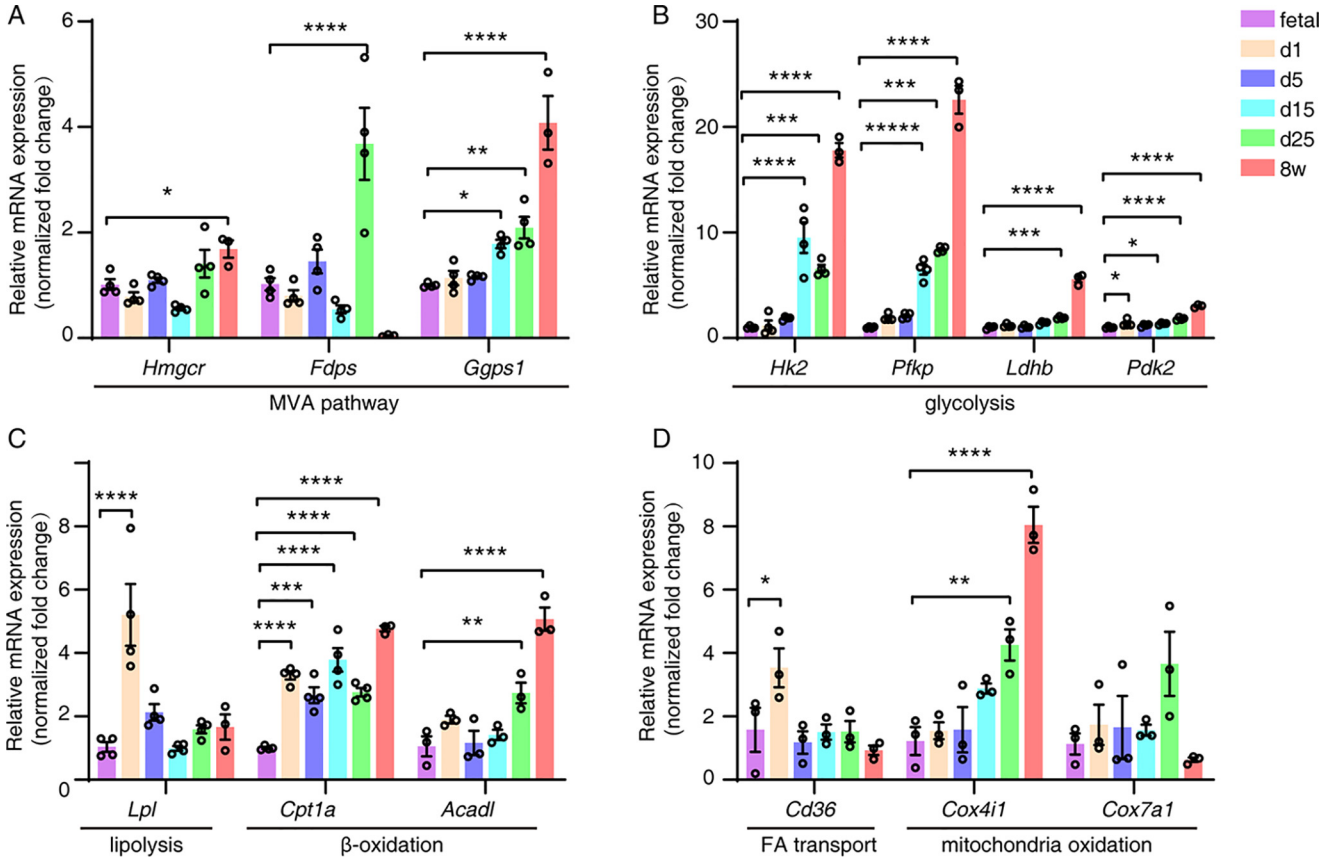

Figure 1. Dynamic expression of the genes associated with metabolism in aorta tissues. *A*, the relative mRNA levels of the genes associated with MVA pathway ($n = 4$). *B*, relative mRNA levels of glycolysis-associated genes ($n = 4$). *C*, relative mRNA levels of lipolysis– and β-oxidation–related genes ($n = 3$). *D*, relative mRNA levels of the genes associated with fatty acid (*FA*) transport and mitochondria oxidation ($n = 4$). The aorta tissues were isolated from C57BL/6 mice (embryonic day 18.5 to 8 weeks) and subjected to a real-time PCR assay. Each *n* was composed of 2–9 mice. Relative mRNA levels were normalized to that of the control group, respectively. All data are presented as mean ± S.E. of biologically independent samples with one-way ANOVA followed by Bonferroni's test. *Error bars*, Bonferroni's multiple comparisons test compared with fetal: *, $p < 0.05$; **, $p < 0.01$; ***, $p < 0.001$; ****, $p < 0.0001$. *d1*, 1 day old.

between muscle layers became straight. At 7 weeks after birth, almost no smooth muscle cells were observed, and the elastic lines were straightened entirely (Fig. 3, *E* and *F*). To test whether there was a problem with smooth muscle development, we also tested mesentery contraction function at 4 weeks old. Upon respective treatment with KCl depolarization and NE, the mesentery from 4-week-old KO mice developed significantly smaller force in contrast to CTR mice (KCl: KO (1.641 ± 0.35 mN) *versus* CTR (2.463 ± 0.425 mN), $p < 0.005$; NE: KO (1.78 ± 0.662 mN) *versus* CTR (2.98 ± 0.237 mN), $p < 0.01$). A similar inhibitory effect was also observed when the muscle was treated with U46619 (Fig. 3*A*). The corresponding reduction in the proportion of contraction function with smooth muscle cell decrease suggests a progressive loss of smooth muscle cells in the aorta, which agrees well with the force development.

To characterize the cell death, we measured the broken DNAs with the terminal deoxynucleotidyltransferase-mediated dUTP nick end labeling(TUNEL) method and the protein expression of LC3-II, GASDME, and GASDMD by Western blotting. By 3 weeks after birth, the smooth muscle cells of the mutant aorta had a clear broken DNA signal (Fig. 3*D* and Fig. S2*A*). LC3-II expression both in whole cell and mitochondria fractions (Fig. S2*B*) was significantly increased. As no GASDMD or GASDME proteins expressed in aorta smooth muscle (Fig. S2*C*), the death of the mutant VSMCs was attributable to apoptosis mixed with mitophagy, rather than to pyroptosis.

We then measured the rescue effect of exogenous GGPP *in vitro*. First, we isolated smooth muscle cells from 2-week-old mice and cultured *in vitro*. The CTR cells grew rapidly from the 4th to 5th day, whereas the mutant cells died gradually (Fig. 4*A*). Upon the addition of GGPP to the culture medium, the mutant cells displayed morphology comparable with that of CTR, although the growth velocity was relatively slow (Fig. 4, *A* and *B*). In addition, all of these rescued cells were SMA- and SMMHC-positive (Fig. 4*C*). These results strongly suggested that the apoptosis of the mutant cells was contributed by GGPP depletion. However, the primary cells of the mutant jejunum, airway, and bladder smooth muscles grew in a similar manner as in CTR cells (Fig. S3, *A*–*F*). This phenomenon explained that these smooth muscles were insensitive to GGPPS deletion due to heterogeneous metabolic patterns. However, the relative low KO efficiency of GGPPS in these tissues might contribute to this differential sensitivity also (Fig. 2, *B* and *C*).

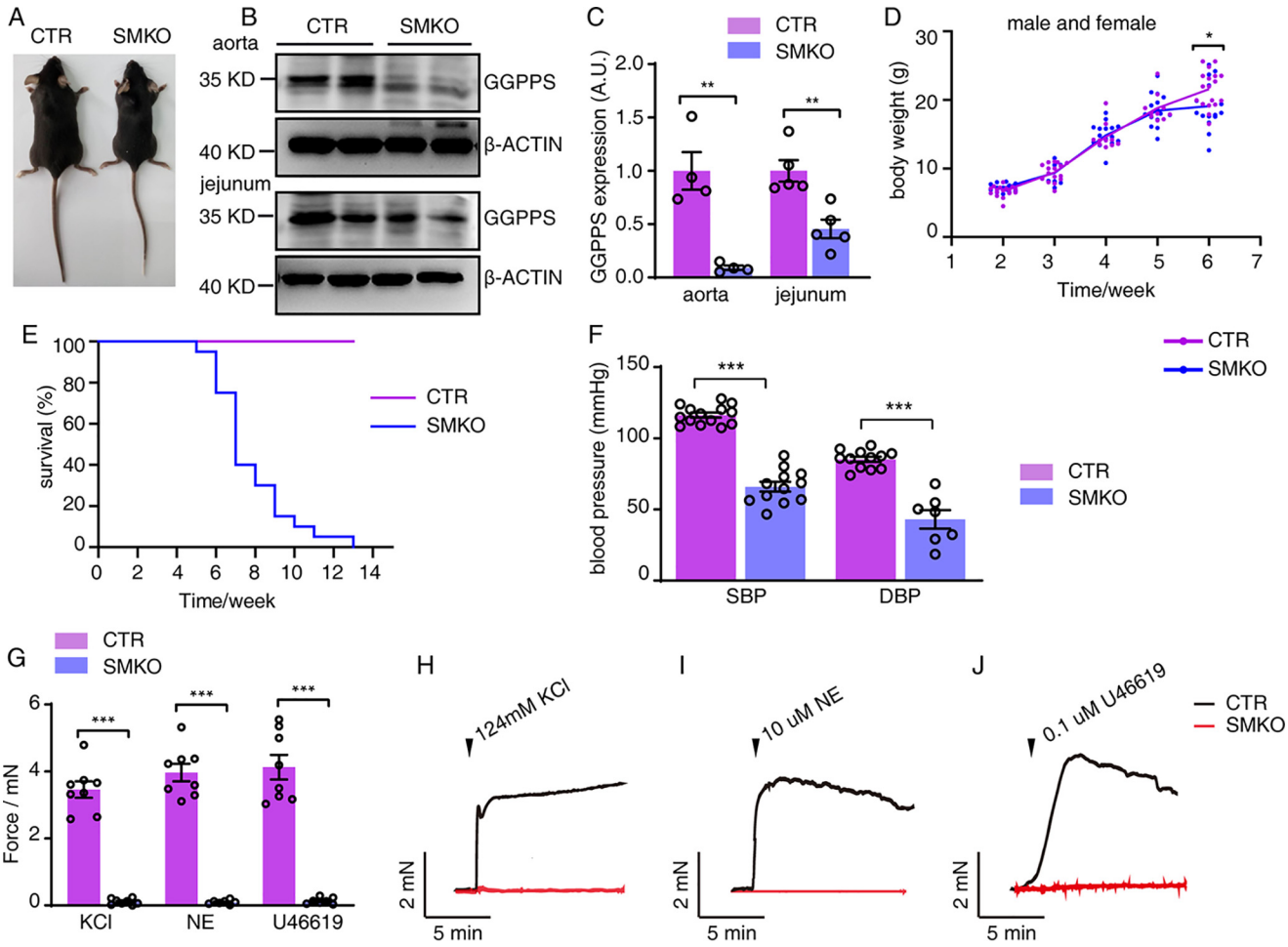

Figure 2. Phenotypic characterization of GGPPS^{SMKO} mice. *A*, schematic representation of the *Ggps1* smooth muscle–specific knockout strategy. *B*, appearance of GGPPS^{SMKO} and CTR mouse. *C* and *D*, Western blotting analysis of GGPPS protein in the aorta and jejunum smooth muscles isolated from 7-week-old GGPPS^{SMKO} and CTR mice. *β*-Actin was employed as a loading control ($n = 5$). *E*, the body weights of GGPPS^{SMKO} mice ($n = 6$–17) and CTR mice. *F*, survival curve of GGPPS^{SMKO} and CTR mice ($n = 20$). *G–J*, the forces of mesentery evoked by 124 mM KCl, 10 μM NE, and 0.1 μM U46619 from 7-week-old mice. $n = 5$ for each group. All data are presented as mean ± S.E. (*error bars*) of biologically independent samples with Student's unpaired *t* test. *, $p < 0.05$; **, $p < 0.01$; ***, $p < 0.001$. *A.U.*, arbitrary units.

GGPPS-deficient vascular smooth muscle displays inflammation responses along with abnormal eicosanoids production

To determine the gene expression profile after GGPPS deletion, we subjected the GGPPS-deficient aorta tissue of 3-week-old mice to RNA-Seq analysis (Table S3). Among 1668 genes with >3-fold altered expression, 1013 genes were up-regulated, and 655 genes were down-regulated. GOTERM function analysis showed that these genes involved 537 pathways or physiological processes. Interestingly, most of them related to innate immunity or inflammation, such as the response to virus, neutrophil chemotaxis, interferon β, and proinflammatory cytokines (*e.g.* interleukin-6, interleukin-1, and tumor necrosis factor) (Fig. 5, *A–C*). This result indicated an apparent metaflammation phenotype after GGPPS deletion. BIOCARTA analysis showed that the altered genes involved cell cycle, eicosanoid metabolism, multiple-drug resistance factors, p53 signaling pathway, classical complement pathway, neutrophil markers, and Ras-independent pathway in NK cell–mediated cytotoxicity (Fig. 5*D*). To further validate the alteration of eicosanoids metabolism, qPCR assays were performed. As expected, the expressions of *Ptgs-1* (also called *Cox-1*), *Cyp2c5*, and *Ptgs-2* (also called *Cox-2*) were changed in the same pattern with the RNA-Seq results (Fig. S4). As eicosanoids are closely related to inflammatory responses (30–35), the metaflammation occurring in the mutant cells may be primarily contributed by the abnormal eicosanoid production.

To learn how eicosanoid metabolism changed, we then examined by the LC–MS method the metabolic products of 53 liposomes related to eicosanoid metabolism (Table S4). Orthogonal partial least-squares discriminant analysis (*O-PLS-DA*) was initially applied to LC–MS data to illustrate separation between KO and control individuals (Fig. 6*A*). The S-plot highlighted four metabolites significantly correlated with GGPPS deficiency (leukotriene B4(LTB4), leukotriene E4(LTE4) instead of LTB4, LTE4, PGE1, and LXA5) (Fig. 6*B*). These dimensionality reduction analyses showed that the metabolite production was significantly changed in GGPPS-deficient aorta smooth muscle (Fig. 6, *A* and *B*) by their change in abundance (Fig. S5). In GGPPS-deficient smooth muscle, such fatty acids as eicosapentaenoic acid (EPA), docosahexaenoic acid (DHA), and arachidonic acid (AA) were accumulated significantly (Fig. 6*C*). Particularly, AA and its intermediate

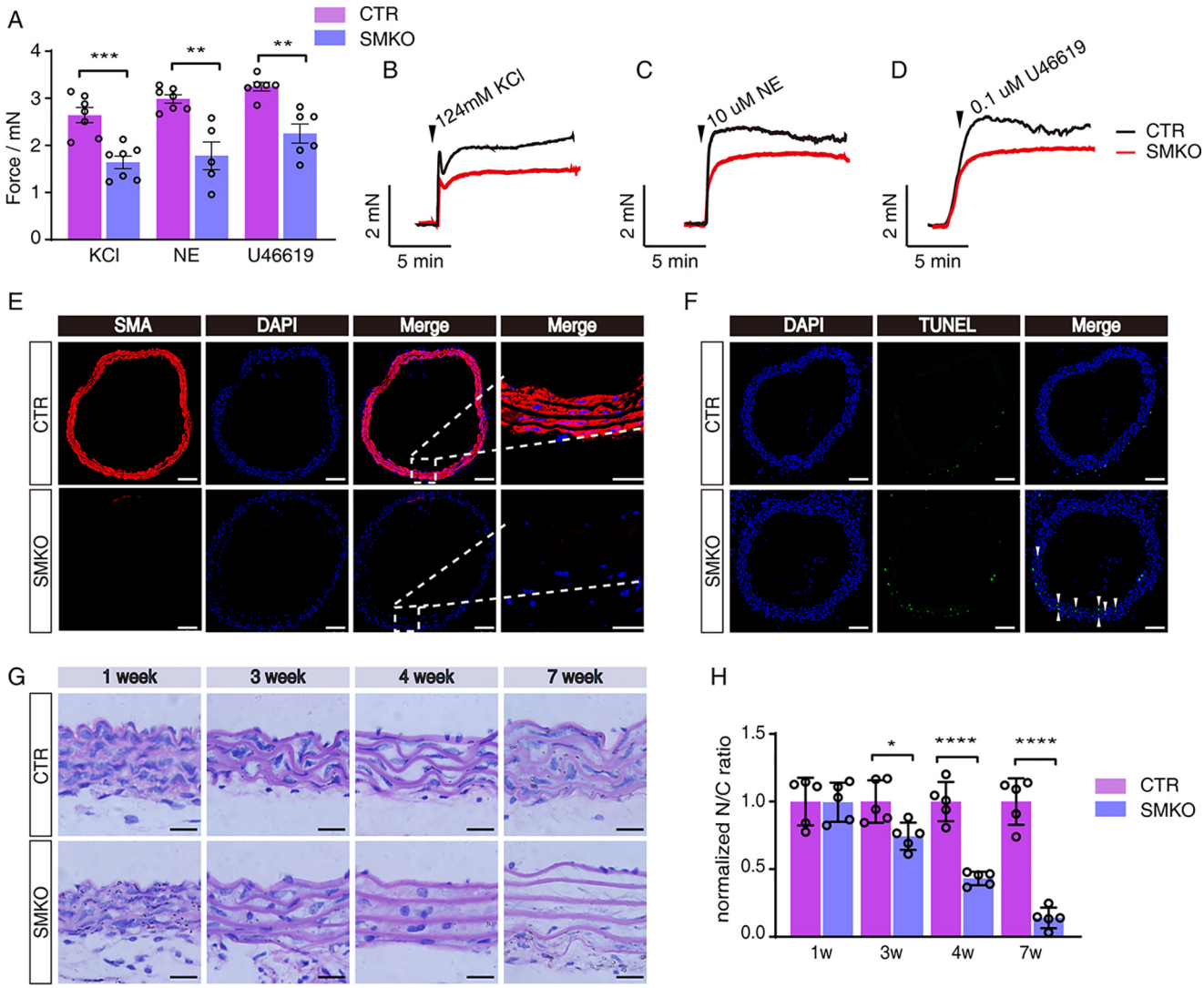

Figure 3. GGPPS deletion significantly impaired neonatal aorta smooth muscle by GGPP depletion. *A–D*, the forces of mesentery evoked by 124 mM KCl, 10 μM NE, and 0.1 μM U46619 from 4-week-old mice. $n = 5$ for each group. *E*, staining smooth muscle cells with anti-SMA antibody and staining nuclei with DAPI dye. *Scale bars*, 25 μm. *Scale bars* in the *magnification frame*, 100 μm. *F*, TUNEL assay for the apoptotic smooth muscle cells from 3-week-old mice. *Scale bar*, 100 μm. $n = 3$ for each group. *White arrow*, apoptotic cells. *G*, HE staining of aorta from 1-week-old ($n = 4$), 3-week-old ($n = 5$), 4-week-old ($n = 5$), and 7-week-old ($n = 6$) mice. *Scale bar*, 20 μm. *H*, quantitation of nucleo-cytoplasmic ratio from *G*. All data are presented as mean ± S.E. (*error bars*) of biologically independent samples with Student's unpaired *t* test. *, $p < 0.05$; **, $p < 0.01$; ***, $p < 0.001$.

products were elevated apparently (*e.g.* LTB4 and LTE4 produced by 5-lipoxygenases (LOXs) were elevated about ~4-fold; the (19*R*)-hydroxy-5*Z*,8*Z*,11*Z*,14*Z*-eicosatetraenoic acid (19-HETE) catalyzed by cytochrome P450 (CYP450) was elevated about ~2-fold; the epoxyeicosatrienoic acids produced by CYP450, including 14,15-epoxyeicosatrienoic acid (EET), 11,12-EET, 8,9-EET, and 5,6-EET, were elevated about ~1.7-fold. The increased liposomes were reported to show proinflammatory tendency, such as chemotaxis of LTB4 (36) and enhanced vascular permeability by LTE4 (37). Therefore, the accumulation of fatty acids or eicosanoids and their bioactive intermediates implies damage to eicosanoid metabolism and thereby inducing inflammation and apoptosis (38).

Given that the accumulated eicosanoids are a pathogenic factor for the inflammation and apoptosis, the neonatal animals in a suckling period would be expected to be more sensitive to GGPPS deletion because abundant polyunsaturated fatty acids existed in mother milk (39), whereas the adult animal would be resistant to GGPPS deletion. To validate this expectation, we crossed *Ggps1*$^{flox/flox}$ mice with SM22-CreERT2 mice and then examined the phenotypes of adult (*Ggps1*^{SM22KO}) mice. After induction with tamoxifen for a week, GGPPS protein level in aorta smooth muscle was reduced to <10% of CTR. However, the survival rate, appearance, and body weights were not altered as we expected. The histology and contractile property of the mutant artery smooth muscle appeared normal also (Fig. S6, *A–F*).

GGPP mediates CYB5R3 translocation from mitochondria to ER through catalyzing CYB5R3 prenylation

To test whether the abnormal eicosanoid production was caused by protein prenylation, we examined the amino acid sequence of the proteins associated with eicosanoids metabolism and found that only CYB5R3 contained a CAA*X* motif in

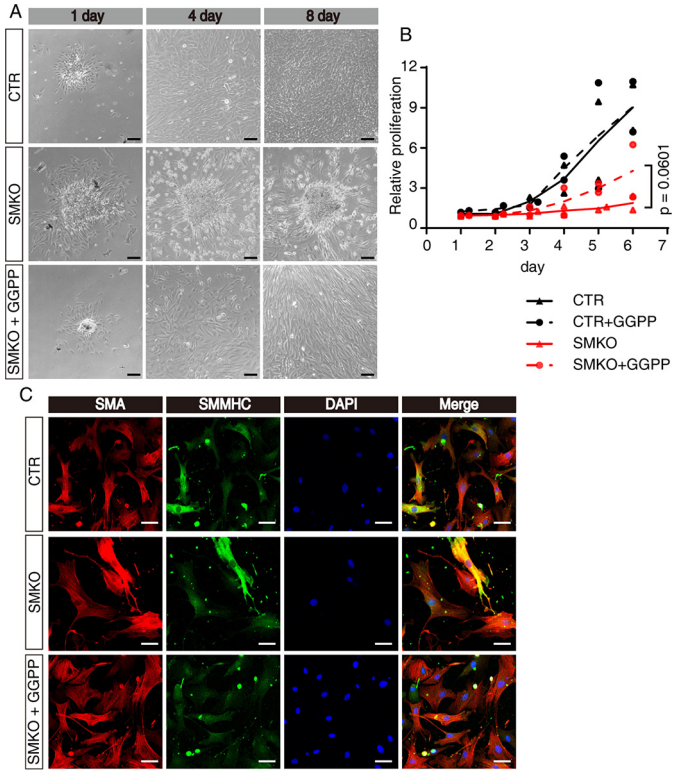

Figure 4. GGPPS deletion significantly impaired neonatal aorta smooth muscle by GGPP depletion. *A*, primary aorta smooth muscle cells isolated from GGPPS^{SMKO} and CTR mice at the age of 14 days were incubated with or without 10 μM GGPP (n = 5). *Scale bars*, 100 μm. *B*, cell proliferation of aorta smooth muscle cells from GGPPS^{SMKO} and CTR mice with or without 10 μM GGPP (n = 3) was tested by CCK-8. *C*, aorta smooth muscle cells were stained with DAPI and smooth muscle marker, SMA and SMMHC (n = 3). *Scale bars*, 50 μm. Data of *B* are presented as mean ± S.E. (*error bars*) of biologically independent samples with two-way ANOVA followed by Bonferroni's test. *ns*, $p > 0.05$; *, $p < 0.05$; **, $p < 0.01$; ***, $p < 0.001$.

the C terminus. CYB5R3 is a reductase using NADH and plasma membrane CoQ as substrates and serves as a key component of the transmembrane redox system (40, 41), which is necessary for redox homeostasis and fatty acid metabolism (42). If CYB5R3 is responsible for the apoptosis of GGPPS-deficient smooth muscle cells, inhibition of CYB5R3 activity should cause smooth muscle apoptosis also. Propylthiouracil (PTU) is a specific (43) and weak inhibitor of CYB5R3 (IC_{50} ~275 μM), and 0.25 mM PTU is sufficient to cause a significant decrease in enzyme activity (44, 45). We treated the primary aorta smooth muscle cells with PTU from 1 to 100 μM. As expected, after incubation with the CYB5R3 inhibitor PTU, the primary aorta smooth muscle cells died in a dose-dependent manner (Fig. 7*A*). We also compared the effect of PTU on A7R5 and primary aortic smooth muscle cells and nonmuscle cells, including CHO cells, RAW 264.7 cells, L929 cells, and 293T cells. 100 μM PTU induced a significant cell death of aortic smooth muscle cells and A7R5 smooth muscle cells, a mild cell death of CHO and RAW 264.7 cells, and no cell death of L929 and 293T cells, implying that smooth muscle was a preferential target of PTU (Fig. S7, *A–F*).

Interestingly, in GGPPS-deficient aorta, the expression of total CYB5R3 protein was elevated (Fig. 7, *B* and *C*), possibly reflecting a compensatory effect secondary to the translocation failure of CYB5R3 as described below. As commercial anti-CYB5R3 antibody just recognizes total CYB5R3 protein, we could not determine whether CYB5R3 was the substrate of GGPP directly. To address this, we made a specific antibody against nonprenylated CYB5R3 (anti-NP-CYB5R3) by immunizing mice with recombinant GST protein fusing with three CAAX motifs of CYB5R3 (Fig. 7*D*). To test the specificity of the anti-NP-CYB5R3 antibody, we applied A7R5 cells transfected with *Cyb5r3* siRNA to a Western blotting assay. After *Cyb5r3* siRNA transfection, the signal produced by anti-NP-CYB5R3 antibody was reduced in the same manner as anti-total-CYB5R3 (Fig. 7*E*). Thus, anti-NP-CYB5R3 appears able to recognize CYB5R3 specifically.

As prenylation enabled protein to anchor on the membrane, we then measured CYB5R3 distribution in the subcellular fractions of A7R5 smooth muscle cells. To our surprise, NP-CYB5R3 was exclusively detected in the mitochondria fraction, whereas total CYB5R3 existed both in mitochondria and plasma membrane (Fig. 7*G*). Treatment with the HMGCR inhibitor simvastatin reduced CYB5R3 protein in the membrane (Fig. 7, *F* and *G*). Therefore, this observation indicated that NP-CYB5R3 was pooled exclusively at mitochondria, whereas prenylated CYB5R3 was pooled at microsome. As the microsomal fraction mainly reflects ER components, the prenylated CYB5R3 is primarily translocated to the ER, the main site for eicosanoid metabolism.

Discussion

Although metaflammation is contributed by signaling networks, it involves a tremendous number of inflammatory cytokines and mediators (2), which etiological factor triggers this inflammation process remains to be determined. In this report, by measuring the role of MVA intermediates in smooth muscle cells, we here found that the inhibition of GGPP led to inflammation through altered production of proinflammatory cytokines, eicosanoids, and other mediators. In light of the fact that MVA or cholesterol biosynthesis is highly affected by other metabolic pathways, such as glycolysis and fatty acid oxidation (46, 47), our findings suggest that the affected MVA pathway may be the etiological pathway triggering metaflammation, in which GGPP serves as a key causal link module. This finding is particularly useful for the development of new anti-metaflammation drugs because it avoids applying multiple targets (48).

This linkage was accomplished by catalyzing CYB5R3 prenylation that was necessary for translocating it from the mitochondria to ER. Prenylation of CYB5R3 was necessary for eicosanoid metabolism (49). As far as we know, CYB5R3 mediates fatty acid elongation and desaturation within the microsomal eicosanoid metabolism. Polyunsaturated fatty acids (*e.g.* AA, EPA, DHA, and linoleic acid) are oxidized by yclooxygenase(COX), lipoxygenase(LOX), cytochrome P450(CYP450) instead of COX, LOX,or CYP450, in which CYB5R3 serves as an electron transfer and maintains oxidation/reduction homeostasis of ER (40, 50, 51). When CYB5R3 is absent or disrupted, the abnormal production of fatty acids is thus induced, which may be sufficient to induce apoptosis of smooth muscle cells. Indeed, CYB5R3 directly participates in CYP450-mediated

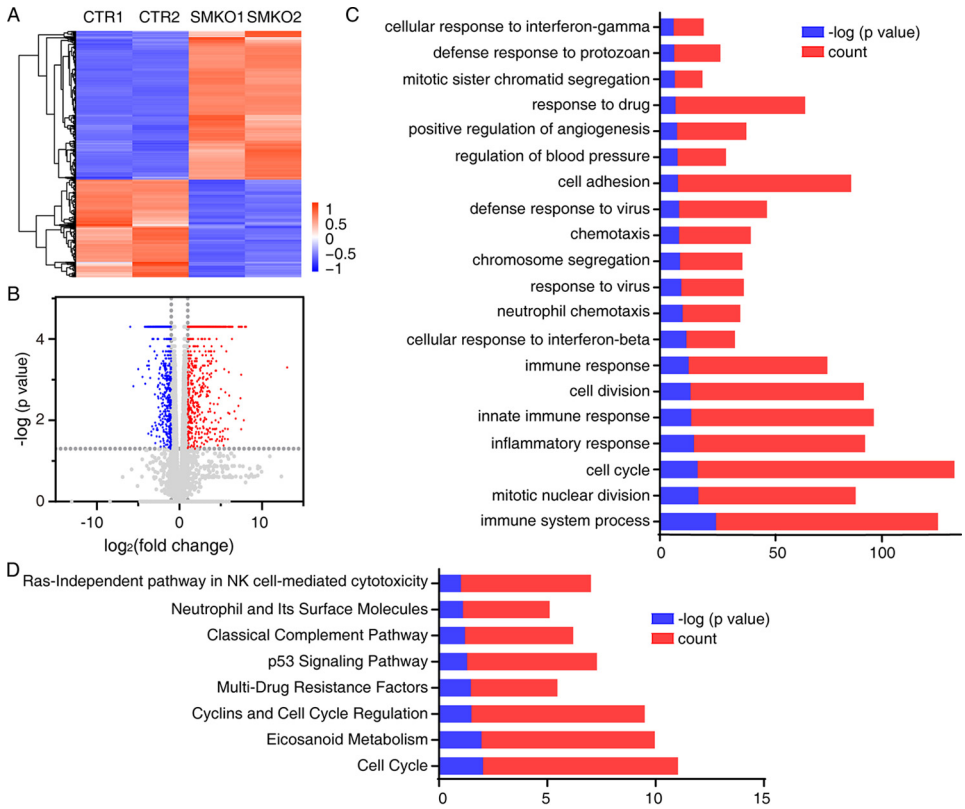

Figure 5. RNA-Seq analysis of GGPPS-deficient aorta. *A*, heatmap of RNA-Seq data from two independent pools from GGPPS^{SMKO} and CTR individuals. *B*, volcano plot of RNA-Seq data from two independent pools from GGPPS^{SMKO} and CTR individuals. *C*, functional category analysis of gene transcripts by GOTERM. *D*, functional category analysis of gene transcripts by BIOCARTA. The data were obtained from two independent pools. 3-Week-old mice were sacrificed, and at least 10 aorta segments were pooled for each independent pool.

hydroxylation, and its absence leads to decreased production of 20-HETE (52). Therefore, our result not only uncovered a regulatory effect of MVA pathway on metaflammation, but also revealed a coordinated regulation of the MVA pathway and eicosanoid metabolism. Moreover, it is also helpful to understand the preferential effect of statin drugs on vascular smooth muscle.

Based on our observations, we proposed a working model (Fig. 8) for the MVA pathway in regulation of inflammation. When mevalonate is produced by ER-docking HMG-CoA, the MVA pathway starts with the participation of mevalonate kinase. As an important member of the isoprenoids, GGPP is synthesized by GGPPS in cytoplasm, and GGTase I/II transfer the resultant GGPP to CYB5R3. The prenylated CYB5R3 translocates from the mitochondrial outer membrane to the ER. The ER-resident CYB5R3 serves to maintain the ER oxidation/reduction balance necessary for such eicosanoid synthesis as microsomal metabolism, or directly participates in the metabolic reactions. When the MVA pathway is inhibited, CYB5R3 prenylation was ablated, and the bioactive intermediate metabolites or substrates of eicosanoid metabolism were accumulated, resulting in metaflammation and death (30, 32–34).

The more interesting finding was that GGPP depletion was specifically detrimental to neonatal mice and not to adult mice. This phenomenon implies that the adult smooth muscle cells of the inducible KO animals are not sensitive to the MVA dysfunction, whereas the perinatal smooth muscle cells are, because 1) the accumulated lipid acids from breast milk are toxic to the smooth muscle cells (SMCs) when they are not metabolized properly (39) and 2) the perinatal SMCs require a large amount of new membrane that is primarily synthesized by cholesterol or the MVA pathway.

The *Cyb5r3* gene encodes for two isoforms in which the soluble isoform is exclusively expressed in erythrocytes and the membrane-bound isoform is expressed in all cells (53, 54). The latter contains a short amino acid sequence (MGAQLSTL) that can be myristoylated and thereby anchor at the membrane. Previous observations have showed that this myristoylated protein simultaneously anchors outside of the mitochondria and ER (54), but the differences existing between the mitochondria and ER forms are not known. Using a specific antibody against NP-CYB5R3, we here found that the NP-CYB5R3 anchored at mitochondria only, whereas the prenylated CYB5R3 anchored at the ER. This means that the *N*-myristoylation event pools the CYB5R3 protein at mitochondria, whereas their further prenylation pools CYB5R3 at ER. This finding uncovered a novel subcellular translocation model of CYB5R3.

In summary, we revealed a mechanistic linkage of MVA with metaflammation and a coupled regulation coordinating MVA with eicosanoid metabolism. The regulatory mechanism underneath involves CYB5R3 prenylation of GGPP that is necessary for microsomal homeostasis and hence eicosanoid metabolism. The

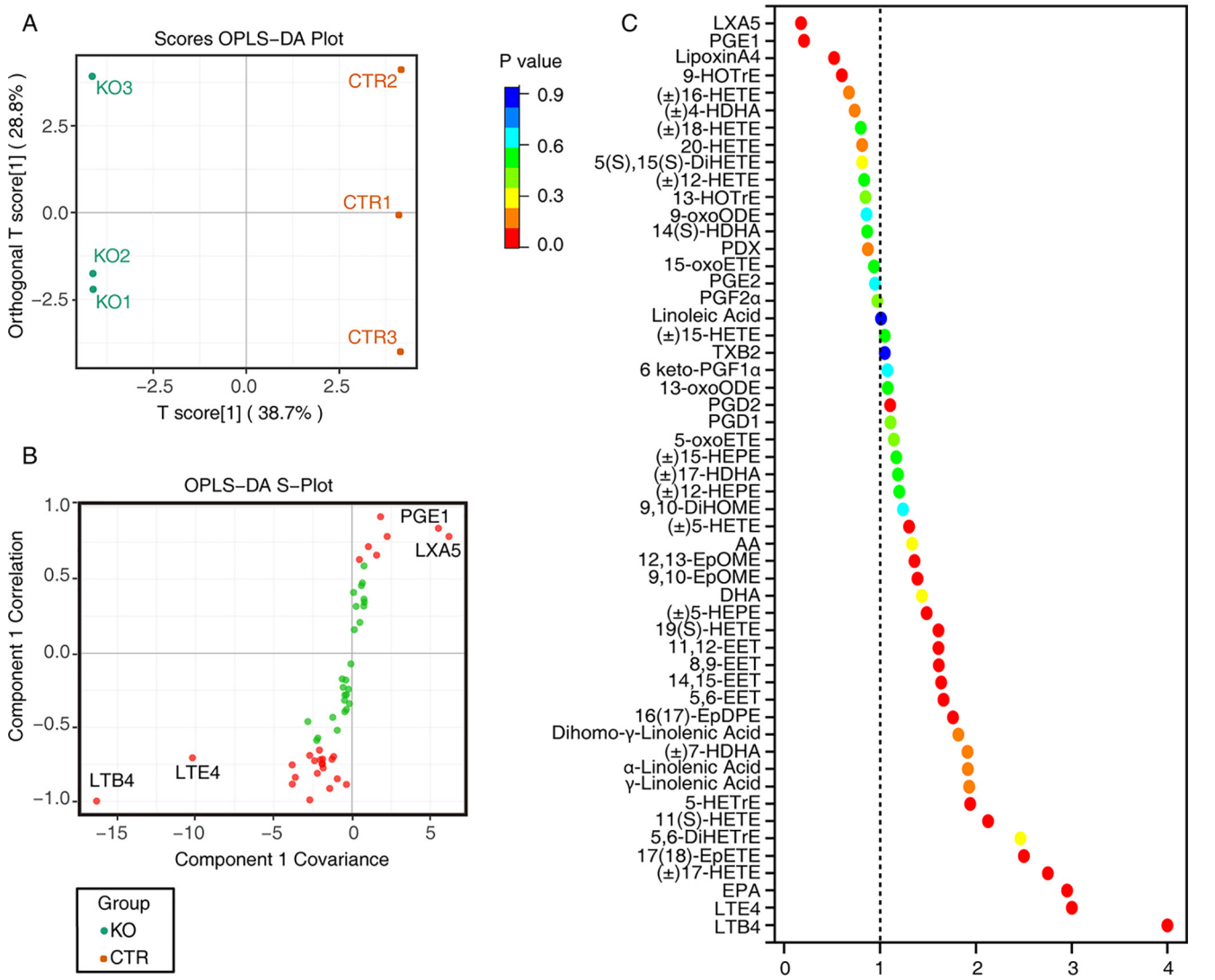

Figure 6. LC–MS analysis of eicosanoids metabolites in GGPPS deficiency aorta. *A*, the orthogonal partial least-squares discriminant analysis (*O-PLS-DA*) score plot illustrates separation between GGPPS^{SMKO} and CTR individuals. *B*, the S-plot indicates the metabolites (highlighted in *red*) showing the highest absolute contribution to the association, with absolute values of covariance or correlation >0.5 or <−0.5. *C*, measurement of the concentration of eicosanoid metabolite–related liposomes in GGPPS^{SMKO} and CTR aorta by LC–MS. The *x* coordinate represents -fold change of SMKO compared with CTR. The data were obtained from three independent pools. Each independent pool was composed of 30 aortas.

MVA pathway or GGPP production is envisioned to be a prospective therapeutic target of metaflammation.

Materials and methods

GGPPS^{SMKO} mice

Floxed *Ggps1* (55) and SMA-Cre (tg) mice (56) were bred and maintained at the Model Animal Research Center of Nanjing University. All animal procedures were performed according to the animal protocol approved by the Institutional Animal Care and Use Committee of the Model Animal Research Center of Nanjing University. All the experiments used both male and female mice.

Primary mouse aorta SMC culture and cell treatment experiment

Primary mouse aorta SMCs were prepared from 2-week-old mice and cultured as described previously (25). Briefly, the aorta was isolated in HT buffer (137.0 mM NaCl, 2.7 mM KCl, 1.8 mM $CaCl_2$, 1 mM $MgCl_2{\cdot}6H_2O$, 5.6 mM D-glucose, and 10 mM HEPES, pH 7.4) and cut longitudinally. All of the following experiments should be performed aseptically. After being washed in D-Hanks' solution (8 g/liter NaCl, 0.0475 g/liter Na_2HPO_4, 0.35 g/liter $NaHCO_3$, 0.4 g/liter KCl, 0.06 g/liter KH_2PO_4), the aorta was cut into small cubes and then digested in 2 mg/ml collagenase I (WLS004196, Worthington) in a 37 °C water bath for 30 min. After being centrifuged at 300 × *g* for 3 min, the tissue pellets were then digested in 2 mg/ml collagenase II (17101015, Gibco) and 0.5 mg/ml elastase (A002290, Worthington). After being centrifuged at 1000 rpm for 3 min, the cell pellets were expanded in high-glucose DMEM containing 10% fetal bovine serum (FBS; Life Technologies), 100 units/ml penicillin, and 100 mg/ml streptomycin and then incubated at 37 °C. For the GGPP rescue experiment, 10 μM GGPP (G6025, Sigma) was added into culture medium once the primary cells were cultured. 1-100 μM propylthiouracil (S1988, Selleck) were incubated with primary aorta SMCs.

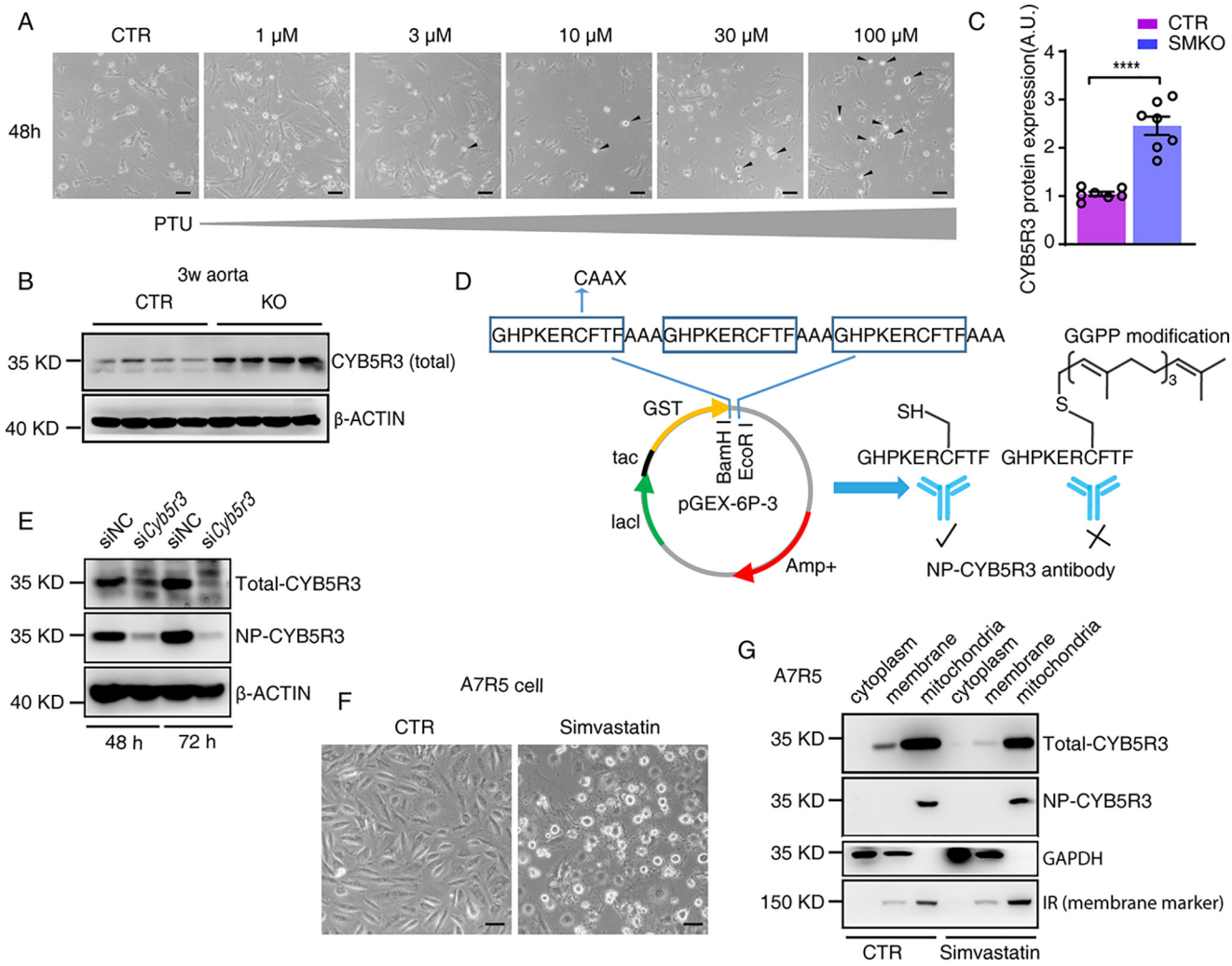

Figure 7. CYB5R3 prenylation of GGPP is required for anchorage at ER. *A*, inhibition of CYB5R3 activity by PTU-induced primary aorta smooth muscle cell death in a dose-dependent manner (n = 3). *Scale bar*, 20 μm. *Black arrow*, dead cells. *B* and *C*, protein expression of CYB5R3 in aorta was increased in 3-week-old GGPPS^{SMKO} mice in contrast to CTR mice (n = 7). *A.U.*, arbitrary units. All data are presented as mean ± S.E. (*error bars*) of biologically independent samples with Student's unpaired t test: ****, $p < 0.0001$. *D*, strategy for making anti-NP-CYB5R3 antibody. A DNA fragment encoding three CAA*X* motifs was inserted into pGEX-6P-3–expressing vector to produce NP-CYB5R3 antibody in BALB/c mice. *E*, CYB5R3 protein was specifically recognized by NP-CYB5R3 antibody. The CYB5R3 expression in A7R5 cells was down-regulated by siRNA transfection. *F*, 10 μM simvastatin induced A7R5 cell death after 24 h *in vitro*. *Scale bar*, 20 μm. *G*, subcellular distribution of NP-CYB5R3 and total CYB5R3 in A7R5 cells. The fractions of cytoplasm, membrane, and mitochondria were isolated from CTR and simvastatin-treated A7R5 cells. CYB5R3 protein was measured by Western blotting with primary antibodies against total CYB5R3 and NP-CYB5R3. GAPDH was used as cytoplasm marker, and insulin receptor (*IR*) was used as membrane marker.

qPCR assay

Quantitative RT-PCR was performed as described previously (29, 57). Briefly, total RNA was extracted from C57BL/6J mice aorta using RNAiso Plus (Takara Bio). Then 1 μg of total RNA was reverse-transcribed with the HiScript® Q RT SuperMix (Vazyme, R123) according to the manufacturer's instructions. Real-time quantitative qPCR was performed using the ABI Prism Step-One system with AceQ® qPCR SYBR® Green Master Mix (Vazyme, R141). The primers for target genes are listed in Table S2. The *36b4* was used as a reference gene.

Western blotting analysis

Tissue was homogenized in modified radioimmune precipitation assay buffer (50 mM Tris-HCl, pH 7.4, 1% Nonidet P-40, 0.25% sodium deoxycholate, 150 mM NaCl, 1 mM EDTA) supplemented with 1× proteinase inhibitor mixture (Roche Applied Science). Protein was quantified with a BCA protein assay kit and then loaded onto SDS-PAGE and transferred to a polyvinylidene difluoride membrane. The membrane was blocked with 5% BSA at room temperature for 1 h and then incubated sequentially with primary and secondary antibodies. The primary antibodies included anti-GGPPS antibody (1:1000; ab155584, Abcam), anti-insulin receptor (1:2000; sc57342, Santa Cruz Biotechnology, Inc.), anti-GASDMD antibody (1:1000; ab209845, Abcam), anti-GASDME antibody (1:1000; ab215191, Abcam), anti-β-actin (1:10,000; AC15, Sigma–Aldrich), anti-GAPDH (1:5000; catalog no. 2133, Signalway), anti-CYB5R3 (1:1000; PA5-36492 (Thermo Fisher Scientific) and 10894-1-AP (Proteintech)), and homemade anti-

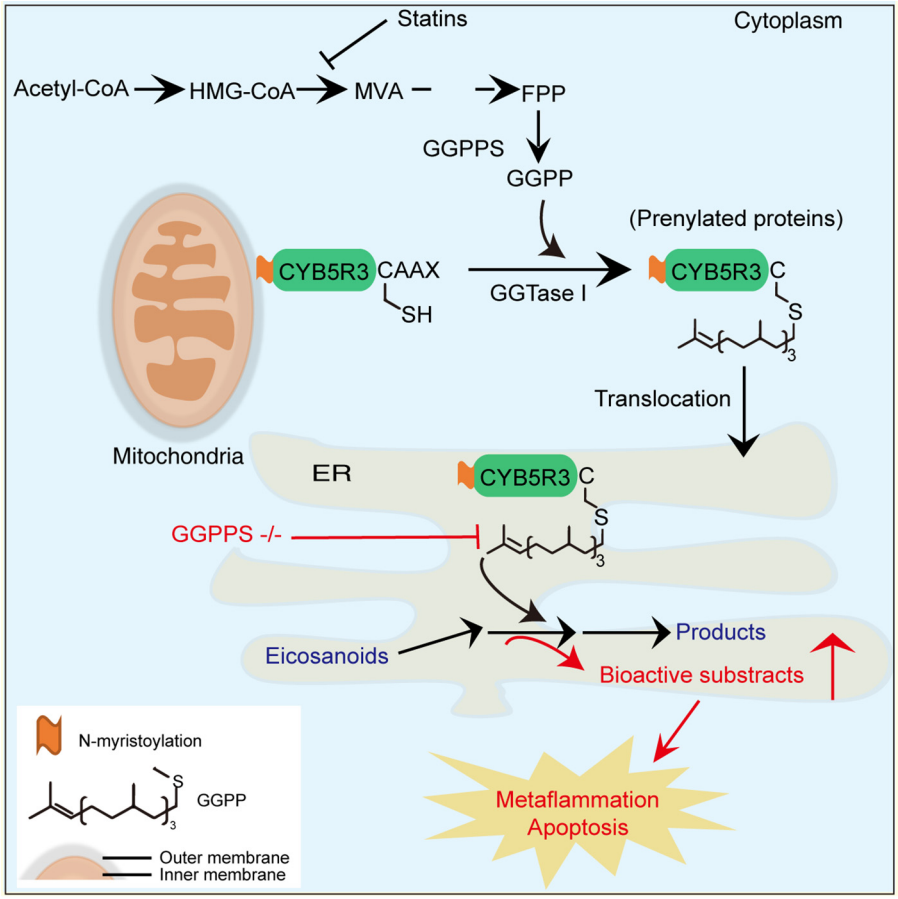

Figure 8. A model for the proposed role of the MVA pathway in triggering of metaflammation. This model suggests that a balance of eicosanoid metabolism is essentially required for neonatal vascular smooth muscle cell survival. Destroyed GGPP prenylation of CYB5R3 impairs eicosanoid metabolism homeostasis.

NP-CYB5R3 antibody (1:1000). The signals were visualized with ECL (Sudgen Biotech).

Blood pressure recording

Blood pressure of mice was measured with a noninvasive tail-cuff method as described previously (25). The mice were fixed in a plastic box on a 37 °C thermostatic blanket. The pulse sensor was placed under the tail of mice (ALC-NIBP system, Shanghai Alcott Biotech). Each mouse took 5 min for adaptation and was measured for 20 cycles with 35-s intervals every day at the regular time. The first 5–7 days were used for training for mice in order to obtain stable recordings. The SBP and diastolic blood pressure were recorded during the next 5–7 days.

Immunofluorescence

The isolated aorta tissues were fixed in 4% paraformaldehyde and then embedded into OCT. The tissues were then sliced into 10-μm thick and incubated with primary antibodies and then incubated with respective secondary antibodies and DAPI (Biosharp). The sections were mounted with 50% glycerol and examined under a Zeiss LSM880 confocal microscope (Zeiss). The primary antibodies were mouse anti-SMA (catalog no. MS-113-P1, Thermo Fisher Scientific) and rabbit anti-SMMHC (ab53219, Abcam).

HE staining

Aorta, mesentery, jejunum, airway, bladder, liver, and heart were isolated and fixed in 4% paraformaldehyde at 4 °C overnight. After ethanol gradient dehydration, the tissues were embedded in paraffin wax and sectioned at a thickness of 5 μm for the following HE stain.

Force measurement of mesentery

Mesentery segments were isolated and subjected to force measurement according to a previous method (58). Briefly, a segment with a length of 1.4 mm was prepared and threaded by two steel wires (40 mm in diameter). The steel wires were then mounted in a myograph chamber (610-M; Danish Myo Technology, Aarhus, Denmark), which contained HT buffer at constant 37 °C. Before stimulation with 124 mM KCl (15.7 mM NaCl, 124.0 mM KCl, 1.8 mM $CaCl_2$, 1 mM $MgCl_2 \cdot 6H_2O$, 5.6 mM D-glucose, and 10 mM HEPES, pH 7.4), the segment was equilibrated in optimal resting tension for 30 min. After washing with HT buffer, the segments were than stimulated with 10 μM norepinephrine (NE) (74490, Sigma) or 0.1 μM U46619 (D8174, Sigma). All forces were persistent for 10 min and recorded on a recording device (AD Instruments, Australia). The data were acquired and analyzed with the LaboratoryChart 5 program.

Apoptosis detection

Aorta frozen sections were subjected to the TUNEL Bright-Green Apoptosis Detection Kit (A112, Vazyme) following the manufacturer's instructions. The cell nucleus was stained with DAPI.

Cell proliferation assay

10 μl of CCK-8 (20148, Sudgen Biotech) was added to each well of cells and incubated at 37 °C for 4 h. Absorbance values at 450 and 650 nm were recorded using a microplate reader (BioTek synergy microplate reader).

Mitochondria isolation

Mitochondria of aorta were isolated as described previously (57). Briefly, the aorta was minced and homogenized and then centrifuged at 600 $\times$ *g* at 4 °C for 15 min twice. The resultant supernatants were centrifuged twice at 8000 $\times$ *g* at 4 °C for 15 min, and the pellet was suspended in MIM buffer (300 mM sucrose, 10 mM Na-HEPES, 0.2 mM EDTA, pH 7.2).

A7R5 cell culture and siRNA of Cyb5r3

Double-stranded siRNA targeting rat *Cyb5r3* was synthesized (GenePharma) with the following sequences: sense, 5′-GGAAAUGAAAGGUAAACAGUU-3′; antisense, 5′-CUGUUUACCUUUCAUUUCCUU-3′. When cell density was up to 1 $\times$ 10^6, 30 nM siRNAs of CYB5R3 or NC were transfected into A7R5 cells using Nucleofection™ 2b (Lonza) with the program X-001 according to the manufacturer's instructions. Cells were lysed with modified radioimmune precipitation assay buffer after 48 and 72 h for protein extraction. For the subcellular fractionation experiment, 10 μM simvastatin (S1792, Selleck) was added to the culture medium.

RNA-Seq analysis

Transcriptomics analysis of 3-week-old mice were performed as described previously (57). Total RNA was isolated from the aorta using RNAiso Plus (Takara Bio). 2 μg of total RNA was sent to a commercial company, Novogene (Beijing, China), for RNA sequencing. Two independent KO samples *versus* CTR mice were analyzed. Paired-end, 150-nucleotide reads were obtained on an Illumina X Ten from the same sequencing lane. The sequencing data were initially processed by Trimmomatic 0.36 and then aligned to the mouse genome UCSC mm10. The aligned results were further assembled using TopHat 2.0.14 with the default parameters and calculated FPKM (fragments per kb of exon per million mapped reads) using Cufflinks version 2.2.1. Gene expression with FPKM $<$1 was excluded in both CTR and KO. KO mice genes with -fold change $>$3-fold compared with CTR and with a significant *p* value ($<$0.05) (a total of 1688 genes) were uploaded into DAVID Bioinformatics Resources 6.8 (RRID:SCR_001881) for GOTERM analysis and BIOCART analysis.

Lipidosome metabolomics analysis

Aorta samples were sent to a commercial company, Metware (Wuhan, China), for lipidosome metabolomics analysis according to, here is the company's official experimental method. Briefly, all experiments were performed on ice. 50 mg of sample and one steel ball were added to 1 ml of methanol. After homogenization for 1–2 min, the steel ball was carefully removed. The samples were whirled for 5 min and then kept still. 10 μl of 1 μM internal standard mixture was added to each sample and vortexed for 10 min. After centrifugation at 5000 rpm for 10 min at 4 °C, the supernatant was blown dry with N_2 and vortexed with 4 ml of a 10% methanol-water mixture. After the SPE column (C18 column) was activated, acid sample was obtained through pH adjustment and quickly added to the SPE column. The target samples were eluted and collected. The collected samples were blown dry with N_2 and then vortexed in 100 μl of methanol-water (1:1, v/v) for 30 s. The supernatants were then analyzed by ultra-high performance liquid chromatography (UPLC; Shim-pack UFLC SHIMADZU CBM30A) and tandem MS (MS/MS; Applied Biosystems QTRAP). The absolute concentrations of target metabolite were calculated based on the standard curves.

Preparation of anti-NP-CYB5R3(292–301) antibody

Anti-NP-CYB5R3(292–301) antibody was prepared as described previously (59). Briefly, GGCCATCCCAAGGAGCGATGCTTCACCTTCGGTGGTGGTGGCCATCCCAAGGAGCGATGCTTCACCTTCGGTGGTGGTGGCCATCCCAAGGAGCGATGCTTCACCTTCGGTGGTGGTTAA was inserted into pGEX6P-3 vector through BamHI and EcoRI. GST–CYB5R3(292–301) was expressed in *Escherichia coli* BL21 (DE3) cells after they were induced with 0.1 mM isopropyl 1-thio-β-D-galactopyranoside. GST–CYB5R3 (292–301) protein was purified with GSH Sepharose 4B (17-0756-01, GE Healthcare) using the gravity flow method according to the manufacturer's instructions. Protein concentrations were measured with a Bio-Rad protein assay kit (500-0006, Bio-Rad). The recombinant protein mixed with Freund's adjuvant (complete: F5881 (Sigma); incomplete: F5506 (Sigma)) was intraperitoneally injected to BALB/c mice for antibody production.

Subcellular fractionation

A7R5 cells were scraped into 500 μl of subcellular fractionation buffer (20 mM HEPES, pH 7.4, 10 mM KCl, 2 mM $MgCl_2$, 1 mM EDTA, 1 mM EGTA, 1 mM DTT) and 1$\times$ proteinase inhibitor mixture (Roche Applied Science) (60). The ice-cold samples were centrifuged at 3000 rpm at 4 °C for 5 min, and the supernatant was subjected to a further centrifugation at 8000 rpm at 4 °C for 5 min. The pellet containing mitochondria was washed with 500 μl of subcellular fractionation buffer one time and lysed in 100 μl of TBS, 0.1% SDS. The supernatant was transferred to a new tube and centrifuged in an ultracentrifuge at 40,000 rpm at 4 °C for 1.5 h. The pellet (membrane fraction) was lysed in 100 μl of TBS, 0.1% SDS. The proteins in all fractions were analyzed by Western blotting.

$GGPPS^{SM22KO}$ mice

The protocol was described previously (61). Floxed *Ggps1* mice were crossed with SM-CreERT2 (ki) mice whose Cre

recombinase is driven by the SM22 promoter. The gene deletion was induced by intraperitoneal injection with tamoxifen (100 μl of 10 mg/ml; Sigma, T5648) for 5 consecutive days at 5 weeks old. 100 mg of tamoxifen was dissolved in 0.5 ml of ethanol at 55 °C and then added with 9.5 ml of sunflower oil and then aliquotted and stored at −80 °C.

Primary jejunum SMC culture

Primary mouse jejunum SMCs were prepared from 2-week-old mice and cultured as described previously (61). The mesentery and adipose tissues were removed. Smooth muscles were carefully teased away from the epithelium. The muscle layers were washed in D-Hanks' solution five times and then cut about 300 times in DMEM with 10% FBS and then digested in 2 mg/ml collagenase II (17101015, Gibco) in a 37 °C water bath for 30 min. After centrifugation at 1000 rpm for 5 min, jejunum SMCs were cultured in DMEM with 10% FBS, 100 units/ml penicillin, and 100 mg/ml streptomycin and then incubated at 37 °C.

Primary airway SMC culture

2-Week-old mice were sacrificed by cervical dislocation. Trachea and extrapulmonary bronchus were isolated, and connective tissues and cartilage were thoroughly removed. Airway smooth muscle was cut and washed in D-Hanks' solution five times. The muscle was then cut about 300 times in DMEM with 10% FBS, 2 mg/ml collagenase I (WLS004196, Worthington), and 1.5 mg/ml trypsin (TB0627, BBI) and digested in a 37 °C water bath for 30 min. After centrifugation at 1000 rpm for 5 min, airway SMCs were cultured in DMEM with 10% FBS, 100 units/ml penicillin, and 100 mg/ml streptomycin at 37 °C.

Primary bladder SMC culture

2-Week-old mice were killed by cervical dislocation (62). The bladder was isolated. The vessel and related tissues were removed. The smooth muscle layers were teased away from the epithelium carefully and washed in D-Hanks' solution five times. The muscle was then cut 300 times in DMEM with 10% FBS and 2 mg/ml collagenase IV (Gibco, 17104019) and 2 mg/ml Dispase II (13783200, Roche Applied Science) and digested in a 37 °C water bath for 40 min. After centrifugation at 1000 rpm for 5 min, bladder SMCs were cultured in DMEM containing 10% FBS, 100 units/ml penicillin, and 100 mg/ml streptomycin and then incubated at 37 °C.

Echocardiography

The echocardiography was measured using a Vevo 3100 High-Resolution *In Vivo* Micro-Imaging System (VisualSonics) according to the manufacturer's instructions. Briefly, the mice were settled on a 37 °C platform after being anesthetized by isoflurane in gas form. The chest hair of the mice was removed with a depilatory cream. The degree of anesthesia was adjusted to obtain a stable heart rate of 350 ± 70 beats/min. M-mode echocardiography was conducted with the RMV 30-mHz scan head.

Quantification and statistical analysis

The animal numbers used for all experiments are indicated in the corresponding figure legends. All value data are presented as means ± S.E. Two-tailed unpaired Student's *t* test was applied to comparisons of two groups (CTR *versus* KO). ANOVA was applied to comparisons of multiple groups. OPLS-DA analysis was from a commercial company, Metware. All heatmap analyses were performed using OmicShare tools, a commercial online platform for data analysis. Fold change analysis of eicosanoid metabolites was performed using Origin 2020b. Statistical analysis was performed using GraphPad Prism 8 software. All quantification analysis of Western blotting was performed using ImageJ software. For qPCR, RNA-Seq, and LC–MS l experiments on mice, *n* represents a sample composed of multiple mice. Statistical differences are indicated as follows: *, $p < 0.05$; **, $p < 0.01$; ***, $p < 0.001$.

Data availability

The RNA-Seq data generated in this study are available in the Gene Expression Omnibus repository under accession number GSE142820.

Acknowledgments—We thank all members of the Zhu laboratories for critical discussion and comments on the manuscript. We also thank the Chao-Jun Li laboratory for providing the *Ggps1*-floxed mice and manuscript review. We also thank Zhen-Ji Gan laboratory (Nanjing University) for providing technical support for RNA-Seq analysis.

Author contributions—L. W., C.-J. L., and M.-S. Z. conceptualization; L. W. and M.-S. Z. data curation; L. W., P. W., T. T., and X. C. software; L. W. formal analysis; L. W. validation; L. W., Y.-Y. Z., J. S., Y. L., X. C., Y. S., D. C., W. Z., Y. Z., Y. W., Z. J., T. Q., and X. Z. investigation; L. W. visualization; L. W., P. W., T. T., M.-S. Z., and X. Z. methodology; L. W. and M.-S. Z. writing-original draft; L. W., C.-J. L., M.-S. Z., and X. Z. writing-review and editing; C.-J. L. and M.-S. Z. resources; M.-S. Z. and X. Z. supervision; M.-S. Z. funding acquisition; M.-S. Z. project administration.

Funding and additional information—This work was supported by National Natural Science Foundation of China Grants 31272311 and 31330034 (to M.-S. Z.).

Conflict of interest—The authors declare that they have no conflicts of interest with the contents of this article.

Abbreviations—The abbreviations used are: MVA, mevalonate pathway; GGPP, geranylgeranyl pyrophosphate; GGPPS, geranylgeranyl diphosphate synthase; CYB5R3, cytochrome b_5 reductase 3; EPA, eicosapentaenoic acid; DHA, docosahexaenoic acid; AA, arachidonic acid; LTB4, leukotriene B4; LTE4, leukotriene E4; ER, endoplasmic reticulum; HMG-CoA, 3-hydroxy-3-methylglutaryl-coenzyme A; HMGCR, 3-hydroxy-3-methylglutaryl-coenzyme A reductase; GGTase I/II, geranylgeranyltransferase I/II; VSMC, vascular smooth muscle cell; SMA, smooth muscle α-actin; NE, norepinephrine; SMMHC, smooth muscle myosin heavy chain; PTU,

propylthiouracil; COX, cyclooxygenase; LOX, lipoxygenase; CYP450, cytochrome P450; KO, knockout; CTR, control; SBP systolic blood pressure; DAPI, 4′,6-diamidino-2-phenylindole; mN, millinewtons; TUNEL, terminal deoxynucleotidyltransferase-mediated dUTP nick end labeling; qPCR, quantitative PCR; FBS, fetal bovine serum; HE, hematoxylin and eosin; DMEM, Dulbecco's modified Eagle's medium; ANOVA, analysis of variance; EET, epoxyeicosatrienoic acid; HETE, hydroxyeicosatetraenoic acid; GAPDH, glyceraldehyde-3-phosphate dehydrogenase.

References

1. Hotamisligil, G. S. (2006) Inflammation and metabolic disorders. *Nature* **444,** 860–867 CrossRef Medline
2. Hotamisligil, G. S. (2017) Inflammation, metaflammation and immunometabolic disorders. *Nature* **542,** 177–185 CrossRef Medline
3. Favier, L. A., and Schulert, G. S. (2016) Mevalonate kinase deficiency: current perspectives. *Appl. Clin. Genet.* **9,** 101–110 CrossRef Medline
4. Goldstein, J. L., and Brown, M. S. (1990) Regulation of the mevalonate pathway. *Nature* **343,** 425–430 CrossRef Medline
5. McTaggart, S. J. (2006) Isoprenylated proteins. *Cell Mol. Life Sci.* **63,** 255–267 CrossRef Medline
6. Zhang, F. L., and Casey, P. J. (1996) Protein prenylation: molecular mechanisms and functional consequences. *Annu. Rev. Biochem.* **65,** 241–269 CrossRef Medline
7. Clarke, S. (1992) Protein Isoprenylation and Methylation at Carboxyl-terminal Cysteine Residues. *Annu. Rev. Biochem.* **61,** 355–386 CrossRef Medline
8. Farnsworth, C. C., Seabra, M. C., Ericsson, L. H., Gelb, M. H., and Glomset, J. A. (1994) Rab geranylgeranyl transferase catalyzes the geranylgeranylation of adjacent cysteines in the small GTPases Rab1A, Rab3A, and Rab5A. *Proc. Natl. Acad. Sci. U. S. A.* **91,** 11963–11967 CrossRef Medline
9. Endo, A. (1992) The discovery and development of HMG-CoA reductase inhibitors. *J. Lipid Res.* **33,** 1569–1582 Medline
10. Lane, K. T., and Beese, L. S. (2006) Thematic review series: lipid posttranslational modifications. Structural biology of protein farnesyltransferase and geranylgeranyltransferase type I. *J. Lipid Res.* **47,** 681–699 CrossRef Medline
11. Jiao, Z., Cai, H., Long, Y., Sirka, O. K., Padmanaban, V., Ewald, A. J., and Devreotes, P. N. (2020) Statin-induced GGPP depletion blocks macropinocytosis and starves cells with oncogenic defects. *Proc. Natl. Acad. Sci. U. S. A.* **117,** 4158–4168 CrossRef Medline
12. Mullen, P. J., Yu, R., Longo, J., Archer, M. C., and Penn, L. Z. (2016) The interplay between cell signalling and the mevalonate pathway in cancer. *Nat. Rev. Cancer* **16,** 718–731 CrossRef Medline
13. Jiang, S., Shen, D., Jia, W. J., Han, X., Shen, N., Tao, W., Gao, X., Xue, B., and Li, C. J. (2016) GGPPS-mediated Rab27A geranylgeranylation regulates β cell dysfunction during type 2 diabetes development by affecting insulin granule docked pool formation. *J. Pathol.* **238,** 109–119 CrossRef Medline
14. Tao, W., Wu, J., Xie, B.-X., Zhao, Y.-Y., Shen, N., Jiang, S., Wang, X.-X., Xu, N., Jiang, C., Chen, S., Gao, X., Xue, B., and Li, C.-J. (2015) Lipid-induced muscle insulin resistance is mediated by GGPPS via modulation of the RhoA/Rho kinase signaling pathway. *J. Biol. Chem.* **290,** 20086–20097 CrossRef Medline
15. Chen, W. B., Lai, S. S., Yu, D. C., Liu, J., Jiang, S., Zhao, D. D., Ding, Y. T., Li, C. J., and Xue, B. (2015) GGPPS deficiency aggravates CCl4-induced liver injury by inducing hepatocyte apoptosis. *FEBS Lett.* **589,** 1119–1126 CrossRef Medline
16. Yeh, Y. S., Jheng, H. F., Iwase, M., Kim, M., Mohri, S., Kwon, J., Kawarasaki, S., Li, Y., Takahashi, H., Ara, T., Nomura, W., Kawada, T., and Goto, T. (2018) The mevalonate pathway is indispensable for adipocyte survival. *iScience* **9,** 175–191 CrossRef Medline
17. Munoz, M. A., Jurczyluk, J., Mehr, S., Chai, R. C., Arts, R. J. W., Sheu, A., McMahon, C., Center, J. R., Singh-Grewal, D., Chaitow, J., Campbell, D. E., Quinn, J. M. W., Alexandrov, K., Tnimov, Z., Tangye, S. G., *et al.* (2017) Defective protein prenylation is a diagnostic biomarker of mevalonate kinase deficiency. *J. Allergy Clin. Immunol.* **140,** 873–875e876 CrossRef Medline
18. Munoz, M. A., Jurczyluk, J., Simon, A., Hissaria, P., Arts, R. J. W., Coman, D., Boros, C., Mehr, S., and Rogers, M. J. (2019) Defective protein prenylation in a spectrum of patients with mevalonate kinase deficiency. *Front. Immunol.* **10,** 1900 CrossRef Medline
19. Takata, R., Fukasawa, S., Hara, T., Nakajima, H., Yamashina, A., Yanase, N., and Mizuguchi, J. (2004) Cerivastatin-induced apoptosis of human aortic smooth muscle cells through partial inhibition of basal activation of extracellular signal-regulated kinases. *Cardiovasc. Pathol.* **13,** 41–48 CrossRef Medline
20. Erl, W. (2005) Statin-induced vascular smooth muscle cell apoptosis: a possible role in the prevention of restenosis? *Curr. Drug Targets Cardiovasc. Haematol. Disord.* **5,** 135–144 CrossRef Medline
21. Knapp, A. C., Huang, J., Starling, G., and Kiener, P. A. (2000) Inhibitors of HMG-CoA reductase sensitize human smooth muscle cells to Fas-ligand and cytokine-induced cell death. *Atherosclerosis* **152,** 217–227 CrossRef Medline
22. Glorioso, N., Troffa, C., Filigheddu, F., Dettori, F., Soro, A., Parpaglia, P. P., Collatina, S., and Pahor, M. (1999) Effect of the HMG-CoA reductase inhibitors on blood pressure in patients with essential hypertension and primary hypercholesterolemia. *Hypertension* **34,** 1281–1286 CrossRef Medline
23. Ferrier, K. E., Muhlmann, M. H., Baguet, J.-P., Cameron, J. D., Jennings, G. L., Dart, A. M., and Kingwell, B. A. (2002) Intensive cholesterol reduction lowers blood pressure and large artery stiffness in isolated systolic hypertension. *J. Am. College Cardiol.* **39,** 1020–1025 CrossRef Medline
24. Borghi, C., Dormi, A., Veronesi, M., Immordino, V., and Ambrosioni, E. (2002) Use of lipid-lowering drugs and blood pressure control in patients with arterial hypertension. *J. Clin. Hypertension (Greenwich)* **4,** 277–285 CrossRef Medline
25. Sun, J., Tao, T., Zhao, W., Wei, L., She, F., Wang, P., Li, Y., Zheng, Y., Chen, X., Wang, W., Qiao, Y., Zhang, X. N., and Zhu, M. S. (2019) CPI-17-mediated contraction of vascular smooth muscle is essential for the development of hypertension in obese mice. *J. Genet. Genomics* **46,** 109–118 CrossRef Medline
26. Lin, C. S., Hsieh, P. S., Hwang, L. L., Lee, Y. H., Tsai, S. H., Tu, Y. C., Hung, Y. W., Liu, C. C., Chuang, Y. P., Liao, M. T., Chien, S., and Tsai, M. C. (2018) The CCL5/CCR5 axis promotes vascular smooth muscle cell proliferation and atherogenic phenotype switching. *Cell Physiol. Biochem.* **47,** 707–720 CrossRef Medline
27. Bundy, J. D., Li, C., Stuchlik, P., Bu, X., Kelly, T. N., Mills, K. T., He, H., Chen, J., Whelton, P. K., and He, J. (2017) Systolic blood pressure reduction and risk of cardiovascular disease and mortality: a systematic review and network meta-analysis. *JAMA Cardiol.* **2,** 775–781 CrossRef Medline
28. Huynh, K. (2017) Hypertension: very low achieved SBP increases risk of cardiovascular death. *Nat. Rev. Cardiol.* **14,** 316–317 CrossRef Medline
29. Qiao, Y. N., He, W. Q., Chen, C. P., Zhang, C. H., Zhao, W., Wang, P., Zhang, L., Wu, Y. Z., Yang, X., Peng, Y. J., Gao, J. M., Kamm, K. E., Stull, J. T., and Zhu, M. S. (2014) Myosin phosphatase target subunit 1 (MYPT1) regulates the contraction and relaxation of vascular smooth muscle and maintains blood pressure. *J. Biol. Chem.* **289,** 22512–22523 CrossRef Medline
30. Esser-von Bieren, J. (2017) Immune-regulation and -functions of eicosanoid lipid mediators. *Biol. Chem.* **398,** 1177–1191 CrossRef Medline
31. Tunctan, B., Senol, S. P., Temiz-Resitoglu, M., Guden, D. S., Sahan-Firat, S., Falck, J. R., and Malik, K. U. (2019) Eicosanoids derived from cytochrome P450 pathway of arachidonic acid and inflammatory shock. *Prostaglandins Other Lipid Mediat.* **145,** 106377 CrossRef Medline
32. Ramirez, M. U., Stirling, E. R., Emenaker, N. J., Roberts, D. D., and Soto-Pantoja, D. R. (2018) Thrombospondin-1 interactions regulate eicosanoid metabolism and signaling in cancer-related inflammation. *Cancer Metastasis Rev.* **37,** 469–476 CrossRef Medline
33. Khan, S. A., and Jackson, R. T. (2018) Polyunsaturated fatty acids, inflammation, and metabolic syndrome in South Asian Americans in Maryland. *Food Sci. Nutr.* **6,** 1575–1581 CrossRef Medline

34. Delmastro-Greenwood, M., Freeman, B. A., and Wendell, S. G. (2014) Redox-dependent anti-inflammatory signaling actions of unsaturated fatty acids. *Annu. Rev. Physiol.* **76,** 79–105 CrossRef Medline
35. Wang, W., Yang, J., Zhang, J., Wang, Y., Hwang, S. H., Qi, W., Wan, D., Kim, D., Sun, J., Sanidad, K. Z., Yang, H., Park, Y., Liu, J. Y., Zhao, X., Zheng, X., *et al.* (2018) Lipidomic profiling reveals soluble epoxide hydrolase as a therapeutic target of obesity-induced colonic inflammation. *Proc. Natl. Acad. Sci. U. S. A.* **115,** 5283–5288 CrossRef Medline
36. Lämmermann, T., Afonso, P. V., Angermann, B. R., Wang, J. M., Kastenmüller, W., Parent, C. A., and Germain, R. N. (2013) Neutrophil swarms require LTB4 and integrins at sites of cell death *in vivo*. *Nature* **498,** 371–375 CrossRef Medline
37. Chan, C. C., and Ford-Hutchinson, A. (1985) Effects of synthetic leukotrienes on local blood flow and vascular permeability in porcine skin. *J. Invest. Dermatol.* **84,** 154–157 CrossRef Medline
38. Song, Z., Huang, G., Chiquetto Paracatu, L., Grimes, D., Gu, J., Luke, C. J., Clemens, R. A., and Dinauer, M. C. (2020) NADPH oxidase controls pulmonary neutrophil infiltration in the response to fungal cell walls by limiting LTB4. *Blood* **135,** 891–903 CrossRef Medline
39. Nilsson, A. K., Löfqvist, C., Najm, S., Hellgren, G., Sävman, K., Andersson, M. X., Smith, L. E. H., and Hellström, A. (2018) Long-chain polyunsaturated fatty acids decline rapidly in milk from mothers delivering extremely preterm indicating the need for supplementation. *Acta Paediatr.* **107,** 1020–1027 CrossRef Medline
40. Villalba, J. M., Navarro, F., Córdoba, F., Serrano, A., Arroyo, A., Crane, F. L., and Navas, P. (1995) Coenzyme Q reductase from liver plasma membrane: purification and role in trans-plasma-membrane electron transport. *Proc. Natl. Acad. Sci. U. S. A.* **92,** 4887–4891 CrossRef Medline
41. Navarro, F., Villalba, J. M., Crane, F. L., Mackellar, W. C., and Navas, P. (1995) A phospholipid-dependent NADH-coenzyme Q reductase from liver plasma membrane. *Biochem. Biophys. Res. Commun.* **212,** 138–143 CrossRef Medline
42. Martin-Montalvo, A., Sun, Y., Diaz-Ruiz, A., Ali, A., Gutierrez, V., Palacios, H. H., Curtis, J., Siendones, E., Ariza, J., Abulwerdi, G. A., Sun, X., Wang, A. X., Pearson, K. J., Fishbein, K. W., Spencer, R. G., *et al.* (2016) Cytochrome b_5 reductase and the control of lipid metabolism and healthspan. *NPJ Aging Mech. Dis.* **2,** 16006–16006 CrossRef Medline
43. Kariya, K., Lee, E., Yamaoka, M., and Ishikawa, H. (1984) Selective induction of cytochrome b_5 and NADH cytochrome b_5 reductase by propylthiouracil. *Life Sci.* **35,** 2327–2334 CrossRef Medline
44. Lee, E., and Kariya, K. (1986) Propylthiouracil, a selective inhibitor of NADH-cytochrome b_5 reductase. *FEBS Lett.* **209,** 49–51 CrossRef Medline
45. Neve, E. P. A., Nordling, Å., Andersson, T. B., Hellman, U., Diczfalusy, U., Johansson, I., and Ingelman-Sundberg, M. (2012) Amidoxime reductase system containing cytochrome b_5 type B (CYB5B) and MOSC2 is of importance for lipid synthesis in adipocyte mitochondria. *J. Biol. Chem.* **287,** 6307–6317 CrossRef Medline
46. Seo, E., Kang, H., Choi, H., Choi, W., and Jun, H. S. (2019) Reactive oxygen species-induced changes in glucose and lipid metabolism contribute to the accumulation of cholesterol in the liver during aging. *Aging Cell* **18,** e12895 CrossRef Medline
47. Gruenbacher, G., and Thurnher, M. (2017) Mevalonate metabolism in immuno-oncology. *Front. Immunol.* **8,** 1714 CrossRef Medline
48. Hotamisligil, G. S. (2017) Foundations of immunometabolism and implications for metabolic health and disease. *Immunity* **47,** 406–420 CrossRef Medline
49. Nakamura, M. T., and Nara, T. Y. (2004) Structure, function, and dietary regulation of Δ6, Δ5, and Δ9 desaturases. *Annu. Rev. Nutr.* **24,** 345–376 CrossRef Medline
50. Heppard, E. P., Kinney, A. J., Stecca, K. L., and Miao, G. H. (1996) Developmental and growth temperature regulation of two different microsomal omega-6 desaturase genes in soybeans. *Plant Physiol.* **110,** 311–319 CrossRef Medline
51. Tocher, D. R., Leaver, M. J., and Hodgson, P. A. (1998) Recent advances in the biochemistry and molecular biology of fatty acyl desaturases. *Prog. Lipid Res.* **37,** 73–117 CrossRef Medline
52. Hildebrandt, A., and Estabrook, R. W. (1971) Evidence for the participation of cytochrome b_5 in hepatic microsomal mixed-function oxidation reactions. *Arch. Biochem. Biophys.* **143,** 66–79 CrossRef Medline
53. Borgese, N., D'Arrigo, A., De Silvestris, M., and Pietrini, G. (1993) NADH-cytochrome b_5 reductase and cytochrome b_5 isoforms as models for the study of post-translational targeting to the endoplasmic reticulum. *FEBS Lett.* **325,** 70–75 CrossRef Medline
54. Leroux, A., Mota Vieira, L., and Kahn, A. (2001) Transcriptional and translational mechanisms of cytochrome b_5 reductase isoenzyme generation in humans. *Biochem. J.* **355,** 529–535 CrossRef Medline
55. Xu, N., Guan, S., Chen, Z., Yu, Y., Xie, J., Pan, F. Y., Zhao, N. W., Liu, L., Yang, Z. Z., Gao, X., Xu, B., and Li, C. J. (2015) The alteration of protein prenylation induces cardiomyocyte hypertrophy through Rheb-mTORC1 signalling and leads to chronic heart failure. *J. Pathol.* **235,** 672–685 CrossRef Medline
56. He, W. Q., Peng, Y. J., Zhang, W. C., Lv, N., Tang, J., Chen, C., Zhang, C. H., Gao, S., Chen, H. Q., Zhi, G., Feil, R., Kamm, K. E., Stull, J. T., Gao, X., and Zhu, M. S. (2008) Myosin light chain kinase is central to smooth muscle contraction and required for gastrointestinal motility in mice. *Gastroenterology* **135,** 610–620 CrossRef Medline
57. Fu, T., Xu, Z., Liu, L., Guo, Q., Wu, H., Liang, X., Zhou, D., Xiao, L., Liu, L., Liu, Y., Zhu, M. S., Chen, Q., and Gan, Z. (2018) Mitophagy directs muscle-adipose crosstalk to alleviate dietary obesity. *Cell Rep.* **23,** 1357–1372 CrossRef Medline
58. Sun, J., Yang, G. M., Tao, T., Wei, L. S., Pan, Y., and Zhu, M. S. (2018) Isometric contractility measurement of the mouse mesenteric artery using wire myography. *J. Vis. Exp.* **20,** 58064 CrossRef Medline
59. Tao, T., Sun, J., Peng, Y., Li, Y., Wang, P., Chen, X., Zhao, W., Zheng, Y. Y., Wei, L., Wang, W., Zhou, Y., Liu, J., Shi, Y. S., and Zhu, M. S. (2019) Golgi-resident TRIO regulates membrane trafficking during neurite outgrowth. *J. Biol. Chem.* **294,** 10954–10968 CrossRef Medline
60. Han, Y. M., Bedarida, T., Ding, Y., Somba, B. K., Lu, Q., Wang, Q., Song, P., and Zou, M. H. (2018) β-Hydroxybutyrate prevents vascular senescence through hnRNP A1-mediated upregulation of Oct4. *Mol. Cell* **71,** 1064–1078.e5 CrossRef Medline
61. Chen, C., Tao, T., Wen, C., He, W. Q., Qiao, Y. N., Gao, Y. Q., Chen, X., Wang, P., Chen, C. P., Zhao, W., Chen, H. Q., Ye, A. P., Peng, Y. J., and Zhu, M. S. (2014) Myosin light chain kinase (MLCK) regulates cell migration in a myosin regulatory light chain phosphorylation-independent mechanism. *J. Biol. Chem.* **289,** 28478–28488 CrossRef Medline
62. Zupančič, D., Mrak Poljšak, K., and Kreft, M. E. (2018) Co-culturing porcine normal urothelial cells, urinary bladder fibroblasts and smooth muscle cells for tissue engineering research. *Cell Biol. Int.* **42,** 411–424 CrossRef Medline